Rapid Communications

Spin-1 Kitaev-Heisenberg model on a honeycomb lattice

Xiao-Yu Dong [1,2] and D. N. Sheng[1]

[1]*Department of Physics and Astronomy, California State University, Northridge, California 91330, USA*

[2]*Department of Physics and Astronomy, Ghent University, Krijgslaan 281, 9000 Gent, Belgium*

(Received 16 December 2019; revised 17 May 2020; accepted 20 August 2020; published 8 September 2020)

We study the Kitaev-Heisenberg model with spin-1 local degree of freedom on a honeycomb lattice numerically by the infinite density matrix renormalization group method on a cylinder geometry. By tuning the relative value of the Kitaev and Heisenberg exchange couplings, we obtain the phase diagram with two spin liquid phases and four symmetry-broken phases. We identify that the spin liquid phases are gapless by calculating the central charge at the pure Kitaev points without the Heisenberg interactions. Comparing to its spin-1/2 counterpart, the position and number of gapless modes of the spin-1 case are quite different. Due to the approximate Z_2 local conservations, the expectation value of the Wilson loop operator measuring the flux of each plaquette stays near to 1, and the static spin-spin correlations remain short range in the entire spin liquid phases.

DOI: 10.1103/PhysRevB.102.121102

Introduction. Ever since it was first proposed by Kitaev in 2006 [1], the two-dimensional (2D) Kitaev model and its various extensions have drawn extensive attention both theoretically and experimentally [2,3]. Depending on the relative relations between the exchange couplings in different spatial directions, the system could be a gapless spin liquid or a gapped Z_2 topologically ordered spin liquid. Under a small external magnetic field, the gapless spin liquid will open a gap and change to a non-Abelian topological phase [4–8], while under a strong magnetic field, the system will be in a fully polarized phase with chiral magnon edge states [9]. The existence of a U(1) gapless quantum spin liquid phase is also proposed in an intermediate magnetic field [10–14]. The other extensions, for example, the addition of Heisenberg exchange terms, may lead to different magnetically ordered phases [15–18]. Some candidate materials with signatures of Kitaev physics have also been found [3,19–21], such as α-$RuCl_3$ [22–28], $H_3LiIr_2O_6$ [29], and $A_2IrO_3 (A = \mathrm{Na}, \mathrm{Li})$ [17,30–37], which motivate more studies on various extended Kitaev models with additional couplings as the effective Hamiltonians for realistic materials.

Despite the numerous studies on the spin-1/2 Kitaev model, the spin-1 case is still less explored and has not been fully understood. The examples of spin-1 spin liquid are quite rare in Heisenberg-like spin models. Due to the fact that the quantum fluctuation is reduced with the increasing of local spin, to realize a spin-1 spin liquid phase the Hamiltonian terms giving rise to frustration need to be strong enough to overcome the tendencies of magnetic ordering or other spontaneous symmetry breaking. Most of the current understandings of the spin-1 Kitaev model are based on the symmetry analysis, such as the existence of Z_2 Wilson loop operators and the vanishing of spin-spin correlations beyond nearest neighbors [38,39]. Small size numerical calculations [40] using exact diagonalization suggested that the ground state of the spin-1 Kitaev model is possibly gapless and vortex-free. Unlike the spin-1/2 Kitaev model, there is no exact solution to the spin-1 model, and the nature of the quantum state is far from understood. A recent theoretical paper [41] proposed the relevance of the spin-1 Kitaev spin model to 2D Mott insulators with strong spin-orbit coupling on lattices with edge-shared octahedra, which may be realized in layered transition metal oxides. This work opens the possibility to find the spin-1 spin liquid phases in real materials and makes the theoretical understanding of the spin-1 Kitaev model more urgent and important.

In this work, we numerically study the spin-1 Kitaev-Heisenberg model of a honeycomb lattice on a cylinder geometry using the density matrix renormalization group (DMRG) method. We obtain the phase diagram with different relative values of the Kitaev and Heisenberg exchange couplings. Two spin liquid phases exist around the antiferromagnetic and ferromagnetic pure Kitaev points (with no Heisenberg term), respectively. The other four phases are magnetically ordered with different patterns of spontaneous symmetry breaking. The entanglement spectrum of the spin liquid phases has a degeneracy with different momentum around a cylinder, while the spectrum of the magnetically ordered phases is dominated by the largest Schmidt value. Most importantly, we find that the ground states of the pure Kitaev points are gapless with nonzero central charges, and the position and number of the gapless modes are different from its spin-1/2 counterpart. Furthermore, the expectation value of the Wilson loop operator measuring the flux of each plaquette stays near to 1, and the static spin-spin correlations remain short range in the entire spin liquid phase.

Phase diagram. We consider the spin-1 Kitaev-Heisenberg model on a 2D honeycomb lattice with the Hamiltonian

$$\hat{H} = K \sum_{\langle i,j\rangle_\gamma} \hat{S}_i^\gamma \hat{S}_j^\gamma + J \sum_{\langle i,j\rangle} \hat{\mathbf{S}}_i \cdot \hat{\mathbf{S}}_j, \tag{1}$$

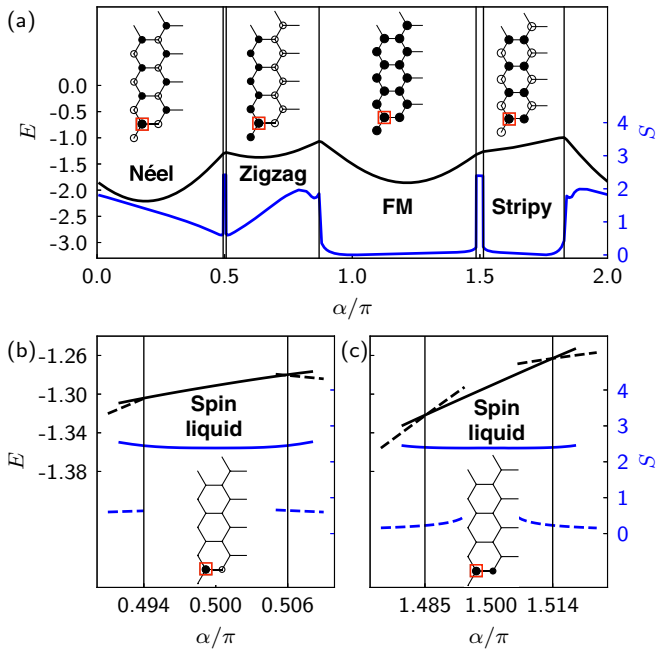

FIG. 1. (a) Phase diagram of the spin-1 Kitaev-Heisenberg model with $\alpha \in [0, 2\pi]$ on an infinite cylinder with $L_y = 4$. The black line is the energy of the ground state per site, and the blue line is the entanglement entropy by cutting the cylinder along a ring. The bond dimension used in iDMRG is $\chi = 1000$. (b) and (c) are the zoom-in plots of the spin liquid phases around $\alpha = 0.5\pi$ and 1.5π, respectively. The black solid lines are the ground state energy per site with calculations initialized in the spin liquid phases, and the black dashed lines are the ground state energy per site with calculations initialized in the corresponding nearby symmetry-broken phases. The blue lines are the entanglement entropy with similar meaning. The phase boundaries are determined by the discontinuous points of the first-order derivatives of the energy of the lowest energy states with respect to α. Insets: The spin-spin correlations $\langle S_i^x S_0^x \rangle$ of each phase in real space with 0 sites marked by the red squares.

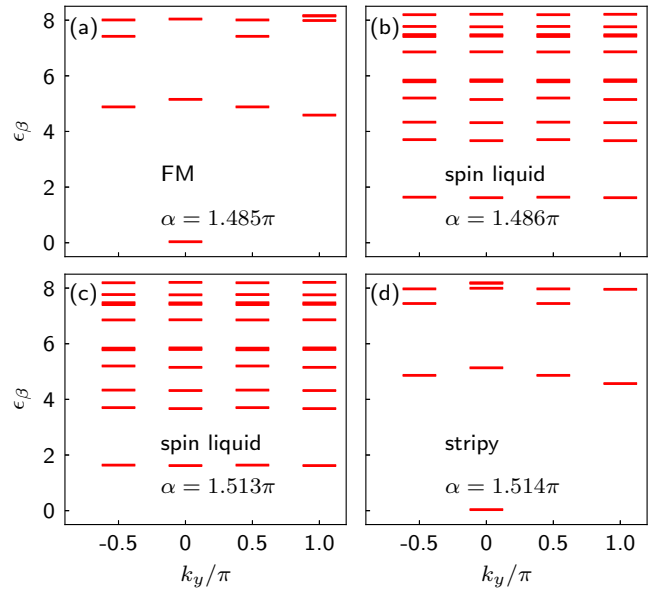

FIG. 2. Entanglement spectrum ϵ_β with momentum k_y around the cylinder of the ground states with (a) $\alpha = 1.485\pi$ in ferromagnetic phase, (b) $\alpha = 1.486\pi$ in spin liquid, (c) $\alpha = 1.513\pi$ in spin liquid, and (d) $\alpha = 1.514\pi$ in stripy phase. All of these α points are the nearest points to the phase transitions in the order of 0.001π.

where $K = 2\sin(\alpha)$ and $J = \cos(\alpha)$ with $\alpha \in [0, 2\pi]$ are the Kitaev and Heisenberg exchange couplings, respectively, $\hat{S}_i^\gamma$ is the γ $(= x, y, z)$ component of the spin-1 operators on site i, and $\langle i, j \rangle_\gamma$ denotes the nearest neighbor coupled by the γ link.

We use an infinite DMRG (iDMRG) method [42,43] on an infinite cylinder with circumference $L_y = 4$ unit cells to get the phase diagram with respect to the parameter α. The translational invariant building block of the infinite cylinder we use has two unit cells in the x direction along the cylinder to be compatible with the symmetry-broken phases. Figure 1(a) shows the phase diagram with the ground state energy per site and the von Neumann entanglement entropy $S = -\sum_\beta \Lambda_\beta^2 \ln \Lambda_\beta^2$, where Λ_β's are the Schmidt values on the bond of the matrix product state (MPS) cutting the infinite cylinder into two halves along a ring. There are four magnetic ordered phases with spontaneous symmetry breaking: Néel phase for α in $[1.83\pi, 2\pi]$ and $[0, 0.494\pi]$, zigzag phase in $[0.506\pi, 0.87\pi]$, ferromagnetic phase in $[0.87\pi, 1.485\pi]$, and stripy phase in $[1.514\pi, 1.83\pi]$, respectively. The insets of Fig. 1(a) give the real-space correlation function $\langle \hat{S}_i^x \hat{S}_0^x \rangle$ for each ordered phase, with 0 sites marked by red squares. The black dot (circle) on each lattice site represents the positive (negative) sign of the correlation and the sizes of the dots and circles are proportional to their absolute values. The spin symmetry-breaking directions of the shown states are along the x direction, i.e., $\langle \hat{S}_i^x \rangle \neq 0$. At $\alpha = 0.5\pi$ and $\alpha = 1.5\pi$, the Heisenberg term $J = 0$, thus the Hamiltonian is pure Kitaev with $K = 2$ and -2, respectively. Two extended spin liquid phases exist around these pure Kitaev points in the region $[0.494\pi, 0.506\pi]$ and $[1.485\pi, 1.514\pi]$ with details shown in Figs. 1(b) and 1(c). In the spin liquids, the quantum frustration from the Kitaev coupling terms dominates, thus no magnetic order appears. The static correlations are short range to the nearest neighbors in the spin liquid as plotted in the insets of Figs. 1(b) and 1(c). The regions of the spin liquid phases are smaller than that of the same model with spin-1/2 [16,44]. The results of iDMRG indicate that the transitions between spin liquid and its nearby symmetry-broken phases are first-order phase transitions. By initializing the calculation from each phase and moving towards the phase transition points, we could find a crossing in the energy lines, as shown by the solid and dashed black lines in Figs. 1(b) and 1(c). This is a key feature of the first-order phase transitions [45].

The entanglement spectrum also shows different structures in the spin liquid and magnetically ordered phases. The cylinder has translational symmetry along the y direction, thus the Schmidt states are eigenstates of the momentum k_y in the y direction and the corresponding entanglement energy levels $\epsilon_\beta = -2 \ln \Lambda_\beta$ can be labeled with k_y. The entanglement spectra near the phase transition point from the ferromagnetic phase to spin liquid are plotted in Figs. 2(a) and 2(b), and from spin liquid to stripy magnetic ordered phase are given in Figs. 2(c) and 2(d). In the ordered phases, the entanglement

spectrum has a nondegenerate dominant value, while in the spin liquid the entanglement spectrum has approximate four-fold degeneracies with different k_y. The abrupt changes of the spectrum structure at the phase transition points are consistent with the first-order phase transitions. We have checked that the spin liquid phases of the spin-1/2 Kitaev model also have similar entanglement structures indicating a strong superposition nature of the spin liquid state.

Pure Kitaev model and spin liquid. In this section we will focus on the pure Kitaev model with $K = \pm 2$ and $J = 0$, and the corresponding spin liquid phases. Let us now review some symmetry properties of the pure Kitaev model. The general Wilson loop operator for spin S on sites $\{1, 2, \ldots, n\}$ of a loop L is defined by

$$\hat{W}_L = e^{i\pi \hat{S}_1^{\gamma_{12}}} e^{i\pi \hat{S}_2^{\gamma_{12}}} e^{i\pi \hat{S}_2^{\gamma_{23}}} e^{i\pi \hat{S}_3^{\gamma_{23}}} \cdots \times e^{i\pi \hat{S}_{(n-1)}^{\gamma_{(n-1)n}}} e^{i\pi \hat{S}_n^{\gamma_{(n-1)n}}} e^{i\pi \hat{S}_n^{\gamma_{n1}}} e^{i\pi \hat{S}_1^{\gamma_{n1}}}, \quad (2)$$

where $\gamma_{i,i+1} (= x, y, z)$ denotes the direction of the link between sites i and $i+1$. It can be verified that $[\hat{W}_L, \hat{H}_K] = 0$ and $[\hat{W}_L, \hat{W}_{L'}] = 0$, where $\hat{H}_K$ denotes the pure Kitaev Hamiltonian. Since $(\hat{W}_L)^2 = 1$, the eigenvalues of $\hat{W}_L$ are $W_L = \pm 1$. We rename $\hat{W}_L$ as $\hat{W}_p$ if the loop is around a single hexagonal plaquette of the honeycomb lattice, and as $\hat{W}_y$ if the loop winds once around the cylinder.

To examine the nature of the spin liquid, we first check if the spin liquid is gapless. We choose two sizes of infinite cylinders with $L_y = 3$ and $L_y = 4$ and consider $\alpha = 1.5\pi$ ($\alpha = 0.5\pi$ is equivalent). We initialize the iDMRG calculations by complex random MPSs with bond dimension $\chi_{\text{ini}} = 100$. A random initial state may give a random bias to help with selecting states in different sectors with different W_y after updating variationally, thus we have a chance to get the lowest energy state in each sector. We name the state with a lower energy of these two states as the ground state and the other one as an excited state.

For $L_y = 3$, the ground state is gapped with $W_y = 1$, while the lowest energy state in the sector with $W_y = -1$ (an excited state) is gapless. For a variational-optimized MPS which represents a gapless state, both the entanglement entropy S and correlation length ξ will increase with its bond dimension, and the scaling relation between them $S = (c/6)\ln\xi$ gives the central charge c of the gapless state. Figure 3(a) shows the finite entanglement scaling for this gapless excited state. The linear fitting (black line) gives the central charge $c \approx 1.097$. The same plot for the gapped ground state is given in the lower right inset of Fig. 3(a). The entanglement entropy of the gapped ground state converges quickly and does not grow with the bond dimension. This observation is quite similar to the spin-1/2 case. In the spin-1/2 case, although with $L_y = 3$ and the periodic boundary condition in the y direction the momentum lines cut through the positions of the gapless Majorana cones at $\pm(\frac{1}{3}, \frac{2}{3})$ in momentum space [see the upper left inset of Fig. 3(a)], the free fermion degree of freedom will adjust to the antiperiodic boundary condition (due to the gauge flux) to give a gapped ground state with lower energy. We conjecture that a similar effect may also play an important role in the spin-1 case as we have seen different flux states ($W_y = \pm 1$) have different central charges on the cylinder with $L_y = 3$. However, due to the lack of an analytical solution,

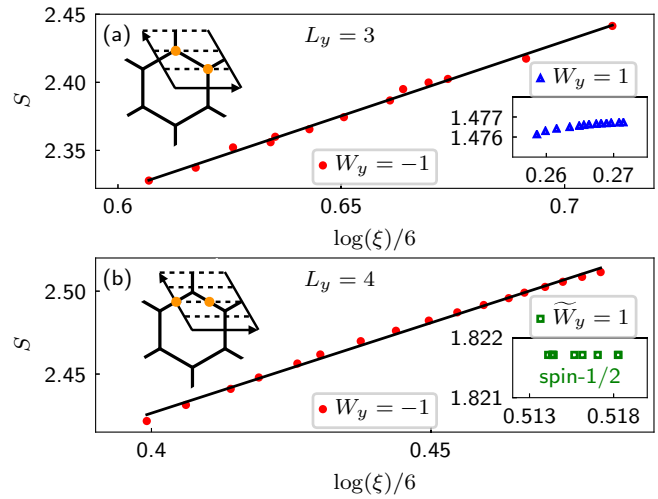

FIG. 3. (a) Finite entanglement scaling of the lowest energy state in the sector with $W_y = -1$ on an infinite cylinder with $L_y = 3$. The bond dimensions of the data points are in the range [500,1200]. The lower right inset is the same plot for the corresponding gapped ground state with $W_y = 1$. (b) Finite entanglement scaling of the ground state with $W_y = -1$ on an infinite cylinder with $L_y = 4$. The bond dimensions of the data points are in the range [1300,2900]. The lower right inset is the same plot for the gapped ground state of the spin-1/2 Kitaev model with $\widetilde{W}_y = 1$ on an infinite cylinder with $L_y = 4$, where $\widetilde{W}_y$ is the corresponding Wilson loop operator around the cylinder for spin-1/2. The slope of the black line in (a) gives the central charge $c \approx 1.097$ and in (b) gives $c \approx 1.088$ by linear fitting with standard deviation errors 0.024 and 0.018, respectively. The upper left insets of (a) and (b) are the Brillouin zone of the honeycomb lattice with $L_y = 3$ and 4, respectively, in which the dashed lines are the momentum lines with periodic boundary condition in the y direction, and orange dots show the possible positions of gapless Majorana cones.

only the results for $L_y = 3$ cannot guarantee if the true ground state in the 2D limit is gapless. Therefore, we consider $L_y = 4$ in the following.

For $L_y = 4$, the ground state of the spin-1 case is gapless and has a fitting central charge $c \approx 1.088$ as shown in Fig. 3(b). This gapless ground state has $W_y = -1$, which is the same as the gapless excited state of $L_y = 3$. The lowest energy state in the sector with $W_y = 1$ is also gapless, but has a larger central charge. This is different from the spin-1/2 case, in which $L_y = 4$ is not compatible with the positions of the Majorana cones, so we always get a gapped ground state as shown in the lower right inset of Fig. 3(b). One possible explanation of the central charge 1 here is that there are two gapless Majorana cones in the spin-1 case, and they may locate at $(0, \frac{1}{2})$ and $(\frac{1}{2}, \frac{1}{2})$ as marked by the orange dots in the upper left inset of Fig. 3(b). We could see that with $L_y = 4$ and the periodic boundary condition in the y direction the momentum lines go through these two points, and give the gapless ground state with central charge $c = 1$ (one Majorana cone contributes 1/2 to the central charge). Notice that the C_6 rotation symmetry is broken by the cylinder geometry, thus the spectrum at $(\frac{1}{2}, 0)$ may be different from that at $(0, \frac{1}{2})$ or $(\frac{1}{2}, \frac{1}{2})$. Other possible situations include gapless excitations

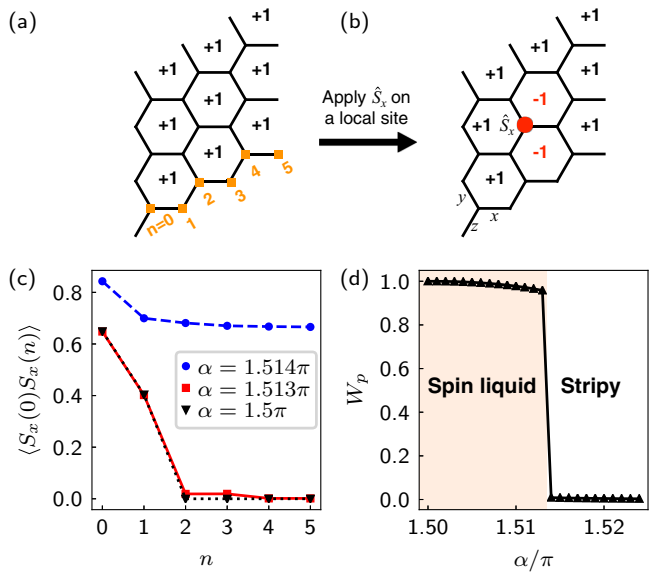

FIG. 4. (a) The real-space lattice with flux $+1$ in each plaquette is schematically shown for the ground state of the pure Kitaev model. The sites $n = 0, 1, \ldots, 5$ with orange squares are used to calculate correlations in (c). (b) Apply $\hat{S}_x$ on one site of the ground state in (a); fluxes in two plaquettes are flipped to -1. (c) The spin-spin correlations $\langle S_0^x S_n^x \rangle$ on n labeled in (a) are plotted at $\alpha = 1.5\pi$, 1.513π, and 1.514π. (d) The flux W_p in each plaquette versus α around the phase transition between spin liquid and stripy phase.

around the $\Gamma = (0, 0)$ point, which is protected by some symmetries, or around a small Fermi sea, which are consistent with both $L_y = 3$ and $L_y = 4$ results.

Besides $\hat{W}_y$, the eigenvalue of local flux operator $\hat{W}_p$ is also a good quantum number of the eigenstates of the pure Kitaev Hamiltonian. The ground states we obtained are vortex-free, i.e., eigenvalues of $\hat{W}_p$ are $+1$ for all of the plaquettes. The flux W_p in each plaquette is near to 1 in the spin liquid phase with $J \neq 0$ around the pure Kitaev points, and drops abruptly to near 0 at the phase transition point as shown in Fig. 4(d).

By direct calculation, we know that $\{\hat{S}_i^\gamma, \hat{W}_p\} = 0$ if site i is on the plaquette p and γ corresponds to one of the two links on p which is connected to site i; otherwise, $[\hat{S}_i^\gamma, \hat{W}_p] = 0$. Therefore, if we apply a local spin operator, for example, $\hat{S}_i^x$ on site i of the lattice, two of the plaquettes which share the site i and link x will reverse their flux W_p as schematically shown in Figs. 4(a) and 4(b). This property leads to the vanishing of the spin-spin correlations beyond the nearest neighbors, since the eigenstates with different quantum number W_p will be orthogonal to each other and thus have zero overlap. This correlation remains short range in the entire spin liquid phase, and changes to long range once the symmetry breaking happens. In Fig. 4(c), the spin-spin correlation $\langle S_0^x S_n^x \rangle$ is plotted with sites $n = 0, 1, \ldots, 5$ as marked in Fig. 4(a), in which $\alpha = 1.5\pi$ is a pure Kitaev point, and $\alpha = 1.513\pi$ and $\alpha = 1.514\pi$ are adjacent to the phase transition point between the spin liquid and stripy phase. We could see that the change of the spin-spin correlation is very sharp crossing the phase transition, and the correlation for the magnetic ordered phase goes to a constant which indicates a long-range-order ground state [46].

Discussion. We identify the gapless spin liquid phases in the spin-1 Kitaev-Heisenberg model, and find that the gapless modes are very different from the corresponding spin-1/2 model. The extensive numerical studies in this work give some insight about the nature of the gapless excitations and could motivate more theoretical studies to fully understand the spin-1 Kitaev model. There are still many open questions about the extended spin-1 Kitaev model for future works. We list a few here: (1) If the Kitaev coupling coefficients are anisotropic, is there a gapped region and what is the topological nature of the gapped phase? (2) If we apply a magnetic field, will the spin liquid open a gap and become a non-Abelian phase? (3) The real materials which realize spin-1 Kitaev coupling may have many other complicated interactions like the spin-1/2 case, so the phase diagram could be much richer. Therefore, more theoretical studies with different coupling terms added to the pure Kitaev model are also interesting.

Note added. Recently, we noticed a related work [47] based on a tensor network approach for the spin-1 Kitaev model. Some conclusions of their work on the nature of spin liquid do not agree with our work, and we believe that further theoretical and numerical studies are needed to resolve the full nature of it.

Acknowledgments. We thank H.-H. Tu, M. Gohlke, R.-Y. Sun, W. Zheng, and Z. Zhu for helpful discussions. iDMRG calculations in this Rapid Communication were performed using the TeNPy Library (version 0.3.0) [43]. Work by X.-Y.D. and D.N.S. were supported by the U.S. Department of Energy, Office of Science, Advanced Scientific Computing Research and Basic Energy Sciences, Materials Sciences and Engineering Division, Scientific Discovery through Advanced Computing (SciDAC) program under the Grant No. DE-AC02- 76SF00515.

[1] A. Kitaev, Anyons in an exactly solved model and beyond, Ann. Phys. **321**, 2 (2006).

[2] M. Hermanns, I. Kimchi, and J. Knolle, Physics of the Kitaev model: Fractionalization, dynamic correlations, and material connections, Annu. Rev. Condens. Matter Phys. **9**, 17 (2018).

[3] J. G. Rau, Eric Kin-Ho Lee, and H.-Y. Kee, Spin-orbit physics giving rise to novel phases in correlated systems: Iridates and related materials, Annu. Rev. Condens. Matter Phys. **7**, 195 (2016).

[4] Z. Zhu, I. Kimchi, D. N. Sheng, and L. Fu, Robust non-Abelian spin liquid and a possible intermediate phase in the antiferromagnetic Kitaev model with magnetic field, Phys. Rev. B **97**, 241110(R) (2018).

[5] L. Zou and Y.-C. He, Field-induced neutral Fermi surface and QCD_3-Chern-Simons quantum criticalities in Kitaev materials, Phys. Rev. Research **2**, 013072 (2020).

[6] H.-C. Jiang, Z.-C. Gu, X.-L. Qi, and S. Trebst, Possible proximity of the Mott insulating iridate Na_2IrO_3 to a

topological phase: Phase diagram of the Heisenberg-Kitaev model in a magnetic field, Phys. Rev. B **83**, 245104 (2011).

[7] L. Janssen, E. C. Andrade, and M. Vojta, Honeycomb-Lattice Heisenberg-Kitaev Model in a Magnetic Field: Spin Canting, Metamagnetism, and Vortex Crystals, Phys. Rev. Lett. **117**, 277202 (2016).

[8] M. Gohlke, R. Moessner, and F. Pollmann, Dynamical and topological properties of the Kitaev model in a [111] magnetic field, Phys. Rev. B **98**, 014418 (2018).

[9] P. A. McClarty, X.-Y. Dong, M. Gohlke, J. G. Rau, F. Pollmann, R. Moessner, and K. Penc, Topological magnons in Kitaev magnets at high fields, Phys. Rev. B **98**, 060404(R) (2018).

[10] H.-C. Jiang, C.-Y. Wang, B. Huang, and Y.-M. Lu, Field induced quantum spin liquid with spinon Fermi surfaces in the Kitaev model, arXiv:1809.08247.

[11] Y.-F. Jiang, T. P. Devereaux, and H.-C. Jiang, Field-induced quantum spin liquid in the Kitaev-Heisenberg model and its relation to α-$RuCl_3$, Phys. Rev. B **100**, 165123 (2019).

[12] S. Liang, M.-H. Jiang, W. Chen, J.-X. Li, and Q.-H. Wang, Intermediate gapless phase and topological phase transition of the Kitaev model in a uniform magnetic field, Phys. Rev. B **98**, 054433 (2018).

[13] C. Hickey and S. Trebst, Emergence of a field-driven $U(1)$ spin liquid in the Kitaev honeycomb model, Nat. Commun. **10**, 530 (2019).

[14] Y. H. Gao, C. Hickey, T. Xiang, S. Trebst, and G. Chen, Thermal Hall signatures of non-Kitaev spin liquids in honeycomb Kitaev materials, Phys. Rev. Research **1**, 013014 (2019).

[15] J. Osorio Iregui, P. Corboz, and M. Troyer, Probing the stability of the spin-liquid phases in the Kitaev-Heisenberg model using tensor network algorithms, Phys. Rev. B **90**, 195102 (2014).

[16] M. Gohlke, R. Verresen, R. Moessner, and F. Pollmann, Dynamics of the Kitaev-Heisenberg Model, Phys. Rev. Lett. **119**, 157203 (2017).

[17] J. Chaloupka, G. Jackeli, and G. Khaliullin, Kitaev-Heisenberg Model on a Honeycomb Lattice: Possible Exotic Phases in Iridium Oxides A_2IrO_3, Phys. Rev. Lett. **105**, 027204 (2010).

[18] E. Sela, H.-C. Jiang, M. H. Gerlach, and S. Trebst, Order-by-disorder and spin-orbital liquids in a distorted Heisenberg-Kitaev model, Phys. Rev. B **90**, 035113 (2014).

[19] S. Trebst, Kitaev materials, arXiv:1701.07056.

[20] S. M. Winter, A. A. Tsirlin, M. Daghofer, J. van den Brink, Y. Singh, P. Gegenwart, and R. Valenti, Models and materials for generalized Kitaev magnetism, J. Phys.: Condens. Matter **29**, 493002 (2017).

[21] G. Jackeli and G. Khaliullin, Mott Insulators in the Strong Spin-Orbit Coupling Limit: From Heisenberg to a Quantum Compass and Kitaev Models, Phys. Rev. Lett. **102**, 017205 (2009).

[22] Y. Kasahara, T. Ohnishi, Y. Mizukami, O. Tanaka, Sixiao Ma, K. Sugii, N. Kurita, H. Tanaka, J. Nasu, Y. Motome *et al.*, Majorana quantization and half-integer thermal quantum Hall effect in a Kitaev spin liquid, Nature (London) **559**, 227 (2018).

[23] K. W. Plumb, J. P. Clancy, L. J. Sandilands, V. V. Shankar, Y. F. Hu, K. S. Burch, H.-Y. Kee, and Y.-J. Kim, α-$RuCl_3$: A spin-orbit assisted Mott insulator on a honeycomb lattice, Phys. Rev. B **90**, 041112(R) (2014).

[24] A. Banerjee, C. A. Bridges, J.-Q. Yan, A. A. Aczel, L. Li, M. B. Stone, G. E. Granroth, M. D. Lumsden, Y. Yiu, J. Knolle *et al.*, Proximate Kitaev quantum spin liquid behavior in a honeycomb magnet, Nat. Mater. **15**, 733 (2016).

[25] S. M. Winter, K. Riedl, P. A. Maksimov, A. L. Chernyshev, A. Honecker, and R. Valentí, Breakdown of magnons in a strongly spin-orbital coupled magnet, Nat. Commun. **8**, 1152 (2017).

[26] A. Little, L. Wu, P. Lampen-Kelley, A. Banerjee, S. Patankar, D. Rees, C. A. Bridges, J.-Q. Yan, D. Mandrus, S. E. Nagler, and J. Orenstein, Antiferromagnetic Resonance and Terahertz Continuum in α-$RuCl_3$, Phys. Rev. Lett. **119**, 227201 (2017).

[27] Z. Wang, S. Reschke, D. Hüvonen, S.-H. Do, K.-Y. Choi, M. Gensch, U. Nagel, T. Rõõm, and A. Loidl, Magnetic Excitations and Continuum of a Possibly Field-Induced Quantum Spin Liquid in α-$RuCl_3$, Phys. Rev. Lett. **119**, 227202 (2017).

[28] K. Ran, J. Wang, W. Wang, Z.-Y. Dong, X. Ren, S. Bao, S. Li, Z. Ma, Y. Gan, Y. Zhang *et al.*, Spin-Wave Excitations Evidencing the Kitaev Interaction in Single Crystalline α-$RuCl_3$, Phys. Rev. Lett. **118**, 107203 (2017).

[29] S. Bette, T. Takayama, K. Kitagawa, R. Takano, H. Takagi, and R. E. Dinnebier, Solution of the heavily stacking faulted crystal structure of the honeycomb iridate $H_3LiIr_2O_6$, Dalton Trans. **46**, 15216 (2017).

[30] J. Chaloupka, G. Jackeli, and G. Khaliullin, Zigzag Magnetic Order in the Iridium Oxide Na_2IrO_3, Phys. Rev. Lett. **110**, 097204 (2013).

[31] S. H. Chun, J.-W. Kim, J. Kim, H. Zheng, C. C. Stoumpos, C. D. Malliakas, J. F. Mitchell, K. Mehlawat, Y. Singh, Y. Choi *et al.*, Direct evidence for dominant bond-directional interactions in a honeycomb lattice iridate Na_2IrO_3, Nat. Phys. **11**, 462 (2015).

[32] S. K. Choi, R. Coldea, A. N. Kolmogorov, T. Lancaster, I. I. Mazin, S. J. Blundell, P. G. Radaelli, Y. Singh, P. Gegenwart, K. R. Choi, S. W. Cheong, P. J. Baker, C. Stock, and J. Taylor, Spin Waves and Revised Crystal Structure of Honeycomb Iridate Na_2IirO_3, Phys. Rev. Lett. **108**, 127204 (2012).

[33] Y. Singh and P. Gegenwart, Antiferromagnetic Mott insulating state in single crystals of the honeycomb lattice material Na_2IrO_3, Phys. Rev. B **82**, 064412 (2010).

[34] Y. Singh, S. Manni, J. Reuther, T. Berlijn, R. Thomale, W. Ku, S. Trebst, and P. Gegenwart, Relevance of the Heisenberg-Kitaev Model for the Honeycomb Lattice Iridates A_2IrO_3, Phys. Rev. Lett. **108**, 127203 (2012).

[35] V. M. Katukuri, S. Nishimoto, V. Yushankhai, A. Stoyanova, H. Kandpal, S. Choi, R. Coldea, I. Rousochatzakis, L. Hozoi, and J. Van Den Brink, Kitaev interactions between $j = 1/2$ moments in honeycomb Na_2IrO_3 are large and ferromagnetic: Insights from *ab initio* quantum chemistry calculations, New J. Phys. **16**, 013056 (2014).

[36] S. C. Williams, R. D. Johnson, F. Freund, S. Choi, A. Jesche, I. Kimchi, S. Manni, A. Bombardi, P. Manuel, P. Gegenwart, and R. Coldea, Incommensurate counterrotating magnetic order stabilized by Kitaev interactions in the layered honeycomb α-Li_2IrO_3, Phys. Rev. B **93**, 195158 (2016).

[37] J. G. Rau, Eric Kin-Ho Lee, and H.-Y. Kee, Generic Spin Model for the Honeycomb Iridates Beyond the Kitaev Limit, Phys. Rev. Lett. **112**, 077204 (2014).

[38] G. Baskaran, D. Sen, and R. Shankar, Spin-S Kitaev model: Classical ground states, order from disorder, and exact correlation functions, Phys. Rev. B **78**, 115116 (2008).

[39] G. Baskaran, S. Mandal, and R. Shankar, Exact Results for Spin Dynamics and Fractionalization in the Kitaev Model, Phys. Rev. Lett. **98**, 247201 (2007).

[40] A. Koga, H. Tomishige, and J. Nasu, Ground-state and thermodynamic properties of an $S = 1$ Kitaev model, J. Phys. Soc. Jpn. **87**, 063703 (2018).

[41] P. P. Stavropoulos, D. Pereira, and H.-Y. Kee, Microscopic Mechanism for a Higher-Spin Kitaev Model, Phys. Rev. Lett. **123**, 037203 (2019).

[42] U. Schollwöck, The density-matrix renormalization group in the age of matrix product states, Ann. Phys. **326**, 96 (2011).

[43] J. Hauschild and F. Pollmann, Efficient numerical simulations with Tensor Networks: Tensor Network Python (TeNPy), SciPost Phys. Lect. Notes **5** (2018), code available from https://github.com/tenpy/tenpy.

[44] See Supplemental Material at http://link.aps.org/supplemental/10.1103/PhysRevB.102.121102 for details.

[45] J. Motruk and F. Pollmann, Phase transitions and adiabatic preparation of a fractional Chern insulator in a boson cold-atom model, Phys. Rev. B **96**, 165107 (2017).

[46] S. Liang, Existence of Néel order at $t = 0$ in the spin-1/2 antiferromagnetic Heisenberg model on a square lattice, Phys. Rev. B **42**, 6555 (1990).

[47] H.-Y. Lee, N. Kawashima, and Y. B. Kim, Tensor network wavefunction of $S = 1$ Kitaev spin liquids, Phys. Rev. Research **2**, 033318 (2020).